Biogeosciences

Mass, nutrient and oxygen budgets for the northeastern Atlantic Ocean

G. Maze[1], H. Mercier[2], V. Thierry[1], L. Memery[3], P. Morin[4], and F. F. Perez[5]

[1]Ifremer, Laboratoire de Physique des Océans, UMR6523, CNRS, Ifremer, IRD, UBO, Plouzané, France
[2]CNRS, Laboratoire de Physique des Océans, UMR6523, CNRS, Ifremer, IRD, UBO, Plouzané, France
[3]CNRS, Laboratoire des sciences de l'Environnement Marin, UMR6539, CNRS, IRD, UBO, Plouzané, France
[4]CNRS, Chimie Marine, UMR7144, AD2M, CNRS & Université Pierre et Marie Curie Paris VI, Place Georges Teissier, 29682 Roscoff, France
[5]Instituto de Investigaciones Marinas (CSIC), Vigo, Spain

Correspondence to: G. Maze (gmaze@ifremer.fr)

Abstract. The northeast Atlantic is a key horizontal and vertical crossroads region for the meridional overturning circulation, but basic nutrient and oxygen fluxes are still poorly constrained by observations in the region. A surface to bottom northeast Atlantic Ocean budget for mass, nutrients (nitrate and phosphate) and oxygen is determined using an optimization method based on three surveys of the OVIDE transect (from Greenland to Portugal) completed with the World Ocean Atlas 2009. Budgets are derived for two communicating boxes representing the northeastern European basin (NEEB) and the Irminger Sea.

For the NEEB (Irminger) box, it is found that 30 % of the mass import (export) across the OVIDE section reach (originate from) the Nordic Seas, while 70 % are redistributed between both boxes through the Reykjanes Ridge $(9.3 \pm 0.7 \times 10^9 \, \text{kg s}^{-1})$.

Net biological source/sink terms of nitrate point to both the Irminger and NEEB boxes as net organic matter production sites (consuming nitrate at a rate of $-7.8 \pm 6.5 \, \text{kmol s}^{-1}$ and $-8.4 \pm 6.6 \, \text{kmol s}^{-1}$, respectively). Using a standard Redfield ratio of $\text{C}:\text{N} = 106:16$, nitrate consumption rates indicate that about $40 \, \text{TgC yr}^{-1}$ of carbon is fixed by organic matter production between the OVIDE transect and the Greenland–Scotland Ridge. Nutrient fluxes also induce a net biological production of oxygen of $73 \pm 60 \, \text{kmol s}^{-1}$ and $79 \pm 62 \, \text{kmol s}^{-1}$ in the Irminger and NEEB boxes, which points to the region as being autotrophic.

The abiotic air–sea oxygen flux leads to an oceanic oxygen uptake in the two regions ($264 \pm 66 \, \text{kmol s}^{-1}$ in the north and $443 \pm 70 \, \text{kmol s}^{-1}$ in the south). The abiotic flux is partitioned into a mixing and a thermal component. It is found that the Irminger Sea oceanic oxygen uptake is driven by an air–sea heat flux cooling increasing the ocean surface oxygen solubility. Over the northeastern European basin the mixing component is about half the thermal flux, presumably because of the oxygen minimum in the subtropical thermocline.

1   Introduction

The northeast Atlantic is a region where subtropical thermocline waters are carried in by the North Atlantic Current (NAC). Those water masses experience strong air–sea interactions and mixing and then either spread toward the Nordic Seas or recirculate westward to the Labrador Sea in the remains of the subpolar gyre (see Fig. 1 in Schott et al., 2004). This surface circulation takes place on top of a deeper one characterized by (i) the mid-depth circulation of Labrador Sea water (Yashayaev et al., 2007; Kvaleberg et al., 2008) and (ii) the southward flow along the flanks of high topographic features – East Greenland shelf and Reykjanes Ridge – of the dense water masses primarily formed in the Nordic Seas and penetrating the northeast Atlantic through the sills between Greenland and Scotland (see Eldevik et al., 2009, and references therein). Intense vertical mixing occurs

in winter in the Iceland Basin, which results in the formation of subpolar mode waters (Brambilla and Talley, 2008; Brambilla et al., 2008; Thierry et al., 2008; de Boisséson et al., 2010, 2012). Moreover, the Irminger Sea is increasingly thought to be a region of periodic deep convection and mode water formation (Pickart et al., 2003a,b; Yashayaev, 2007; Falina et al., 2007; Sproson et al., 2008; Van Aken et al., 2011). The northeast Atlantic is thus a key horizontal and vertical crossroads region where strong air–sea interactions are at the origin of part of the deep water masses feeding the lower branch of the meridional overturning circulation.

However, most of the attention has been toward the circulation of mass, heat and salt while basic nutrient and oxygen fluxes are still poorly constrained by observations in the region. One noticeable exception is the study by Álvarez et al. (2002), who derived nitrate/nitrogen and oxygen budgets for the northeast Atlantic region north of the WOCE A25 4× section between Greenland and Portugal. However, their mass transport estimates have been improved (Lherminier et al., 2007) so that their tracer transports have to be revisited, which will be done in this study. Oceanic nutrient and oxygen fluxes are useful quantities to improve our comprehension of the global carbon cycle. On one hand oceanic anthropogenic carbon fluxes and storage are determined knowing the natural carbon fluxes, which can be inferred from oxygen and nutrient fluxes and budget (Álvarez et al., 2003). On the other hand air–sea oxygen fluxes are necessary to differentiate the ocean and land sinks of the atmospheric anthropogenic carbon (Bopp et al., 2002). This study is thus an attempt to provide estimates of nutrient and oxygen fluxes constrained by observations.

Over the past decade, every two years from 2002 to 2010, the OVIDE project (http://www.ifremer.fr/lpo/ovide/) performed a Greenland to Portugal high-resolution hydrographic survey (about 40 km between each stations). All cruises sampled high quality measurements of standard tracers such as temperature, salinity, nitrate, phosphate and oxygen. Each R/V *rosette* was equipped with an Acoustic Doppler Current Profiler (ADCP), and each survey thus provides a velocity field estimate from the surface to the bottom. These data were combined with thermal wind velocity estimates from hydrography and with Ekman current estimates from satellite data and optimized in a least square sense by Lherminier et al. (2007, 2010) and Gourcuff et al. (2011) to obtain an accurate absolute velocity field normal to the cruise track. From there, tracer transports and their associated errors can be estimated. The interannual OVIDE dataset is thus a unique opportunity to compute mean accurate tracer transports over more than one year.

In this study we propose to use all available tracer transports to date through the OVIDE path – i.e. 2002, 2004 and 2006 – (2008 and 2010 velocity fields are still undergoing analysis) to compute the 2002–2006 time average. Essentially, we propose to combine these transports with transport estimates through the Greenland–Scotland Ridge – quanti

ties well documented from observations in the literature – to compute mass, nutrient and oxygen budgets for the northeast Atlantic, defined here as the area between the OVIDE path and the Greenland–Scotland Ridge (see Fig. 1).

The paper is organized as follows. Section 2 describes the method, domain and model. In Sect. 3 we analyze the optimized mass, nutrient and oxygen budgets. The air–sea oxygen abiotic flux is decomposed in Sect. 4. Results are discussed in Sect. 5 and we conclude in Sect. 6.

2 Method, domain and model

In the next two sections we describe the domain of analysis, the set of conservation equations (or budgets) used to constrain the circulation, biological source/sink terms and air– sea oxygen fluxes for the northeast Atlantic Ocean and the associated timescale.

It would be possible to compute separately mass, nutrient and oxygen budgets. However, on one hand such budgets could eventually be inconsistent with each other, and on the other hand some of the terms (biological and air–sea fluxes for instance), poorly known, would be *de facto* determined as residuals to close the budgets. Here, we are interested in using a method to reconcile these budgets so that they are all satisfied simultaneously.

This is a classic optimization problem tackled here using a linear inversion procedure described in Appendix A. This method increases the physical and biogeochemical consistency of the system and thus improves our knowledge thereof. The procedure is initialized with an a priori estimate and error bar for each variable to be optimized (those include the budget's residuals). After optimization, error bars are smaller and conservation equations are satisfied within the imposed error bars.

2.1 Geographical domain and timescale

The geographical domain of analysis is represented in Fig. 1a, for which a schematic view is given in the same figure, panel (b). The domain is bounded by the OVIDE survey track (red marks) on the southwestern flank and by the Greenland–Scotland Ridge (GSR, blue marks) on the northeastern flank. We split the domain along the Reykjanes Ridge (RR, black marks) into two boxes: one to the north referred to as the "Irminger" box and one to the south referred to as the "northeastern European basin" (NEEB) box. Both boxes extend vertically from the air–sea interface to the bottom topography. A similar geographical domain was used by Lherminier et al. (2010) to constrain the volume flux across the Reykjanes Ridge. Here, we extend their analysis to nutrient and oxygen fluxes.

Hereafter in the study, variables related to: (i) the Irminger and NEEB boxes are labeled using subscripts "n" and "s", (ii) the vertical westernmost and easternmost faces are
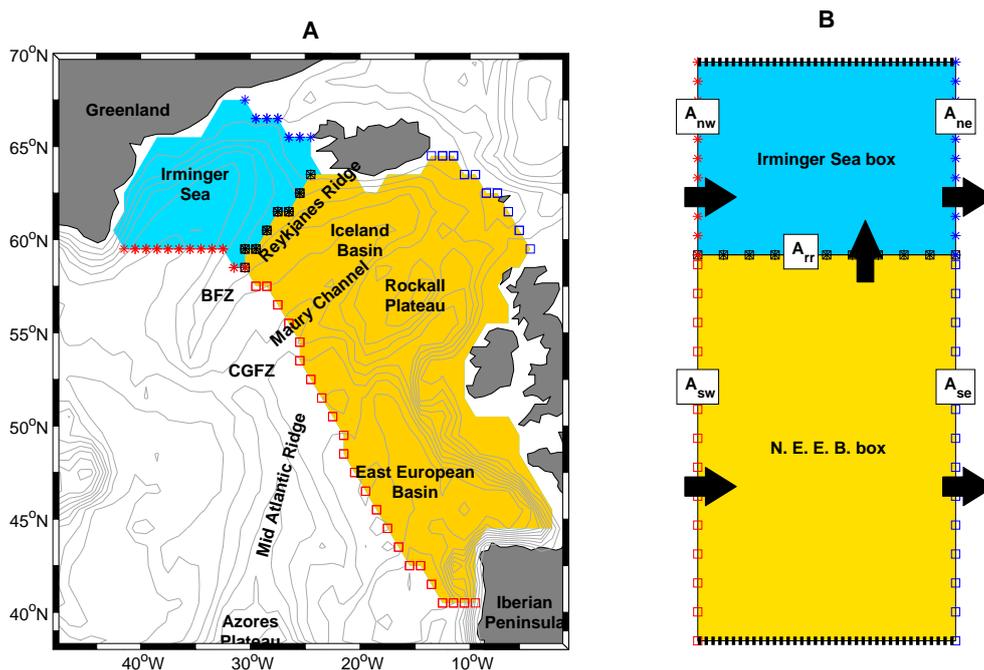
Fig. 1. (A) Localizations of the Irminger Sea (light blue shaded area) and northeastern European basin (NEEB, yellow shaded area) boxes. Main geographic and topographic features are indicated. **(B)** The associated two box model simplified schematic. Black arrows indicate the convention for horizontal positive transports. The white-background labels indicate face labelling convention, here applied to the surface A of faces. Blue/red star/square marks are drawn to help localize faces from panel **(A)** to **(B)**.

Table 1. A priori state estimates of optimized variables.

Variable (unit)	Estimate	±	error	Source
Western face mass transports (based on Eqs. B1–B2, positive: north/eastward)				
$\mathbf{T}_{nw}^{\rho}$ (10^9 kg s^{-1})	−13.3	±	1.5	OVIDE mean 2002,4,6
$\mathbf{T}_{sw}^{\rho}$ (10^9 kg s^{-1})	13.8	±	1.6	Idem
Eastern and RR volume fluxes (positive: north/eastward)				
$\mathbf{F}_{ne}$ (10^6 m^3 s^{-1})	−4.3	±	2.2	IIC + EGC + DSOW
$\mathbf{F}_{se}$ (10^6 m^3 s^{-1})	4.7	±	2.2	ISI + ISOW
$\mathbf{F}_{rr}$ (10^6 m^3 s^{-1})	12.0	±	5.0	Treguier et al. (2005); Bower et al. (2002)
Air–sea abiotic oxygen flux (based on Eq. 10, positive: ingassing)				
$\mathbf{J}_n^a$ (kmol s^{-1})	100	±	200	Twice the annual thermal flux using surface WOA09 monthly climatology combined with OAFlux heat fluxes (Yu et al., 2008)
$\mathbf{J}_s^a$ (kmol s^{-1})	160	±	320	Idem
Biological source/sink term of nitrate (positive: source)				
$\mathbf{B}_n$ (kmol s^{-1})	16.0	±	32.0	Lee (2001) NCP estimates
$\mathbf{B}_s$ (kmol s^{-1})	75.2	±	150.4	Idem

labeled using "w" and "e", (iii) the vertical RR face using "rr", and (iv) the horizontal air–sea interface labeled using "a". Fig. 1b provides an example of this convention to the face area A.

In this study we focus on tracer budgets using the high quality OVIDE dataset. Thus, on the westernmost faces of the domain we used the time mean of OVIDE data for 2002, 2004 and 2006 (Lherminier et al., 2007, 2010; Gourcuff

Table 2. Parameters used to compute budget terms but not optimized by the procedure.

Parameter (unit)	Value	±	error	Source
Western face tracer transports used in Eq. (B3) to compute C_w (positive: north/eastward)				
$T_{nw}^{NO_3}$ (kmol s^{-1})	−187.4	±	23.3	OVIDE mean 2002,4,6
$T_{sw}^{NO_3}$ (kmol s^{-1})	199.1	±	28.5	Idem
$T_{nw}^{PO_4}$ (kmol s^{-1})	−12.2	±	1.5	Idem
$T_{sw}^{PO_4}$ (kmol s^{-1})	12.1	±	1.9	Idem
$T_{nw}^{O_2}$ (kmol s^{-1})	−4089	±	406	Idem
$T_{sw}^{O_2}$ (kmol s^{-1})	3208	±	429	Idem
$T_{nw}^{O_2^s}$ (kmol s^{-1})	−4387	±	460	Idem
$T_{sw}^{O_2^s}$ (kmol s^{-1})	3833	±	515	Idem
Eastern face concentrations (based on the decomposition Eq. C2)				
ρ_{ne} (kg m^{-3})	1028.5			WOA09 annual climatology
ρ_{se} (kg m^{-3})	1028.7			Idem
$C_{ne}^{NO_3}$ (µmol kg^{-1})	12.7			Idem
$C_{se}^{NO_3}$ (µmol kg^{-1})	12.0			Idem
$C_{ne}^{PO_4}$ (µmol kg^{-1})	0.9			Idem
$C_{se}^{PO_4}$ (µmol kg^{-1})	0.8			Idem
$C_{ne}^{O_2^s}$ (µmol kg^{-1})	332.3			Idem
$C_{se}^{O_2^s}$ (µmol kg^{-1})	309.0			Idem
$C_{ne}^{O_2}$ (µmol kg^{-1})	303.4			Idem
$C_{se}^{O_2}$ (µmol kg^{-1})	285.5			Idem
Reykjanes Ridge face concentrations				
ρ_{rr} (kg m^{-3})	1030.7			WOA09 annual climatology
$C_{rr}^{NO_3}$ (µmol kg^{-1})	15.3			Idem
$C_{rr}^{PO_4}$ (µmol kg^{-1})	1.1			Idem
$C_{rr}^{O_2^s}$ (µmol kg^{-1})	302.1			Idem
$C_{rr}^{O_2}$ (µmol kg^{-1})	270.0			Idem

et al., 2011). The relevant timescale for our budget is hence the period 2002–2006.

In order to derive budgets, complementary information about tracers and transports were required at the GSR and along the RR. Unfortunately, direct observations for the period 2002–2006 are not available. We thus used tracer information provided by the World Ocean Atlas (Garcia et al., 2005, WOA09) and transport estimates from the literature (see Appendix B and Tables 1–2). To limit possible inconsistencies due to the asynchronicity of those datasets, we selected the level of error estimates on easternmost face variables to encompass the interannual to decadal variability (Dickson et al., 2008b). This implies that although there is no specific timescale associated with the easternmost face variables used in this study, those values are thought to be compatible within error bars with the 2002–2006 mean value.

The timescale over which budgets described in this study are valid is thus the period 2002–2006.

2.2 Model

The model is a linear set of equations representing mass, nutrient (nitrate and phosphate), oxygen solubility and total oxygen budgets for the Irminger and NEEB boxes as well as their junction. For each of these 3 domains, we write the following 5 equations:

$$0 = \nabla T \tag{1}$$

$$0 = \nabla N\, T + B \tag{2}$$

$$0 = \nabla P\, T + r_{P:N} B \tag{3}$$

$$0 = \nabla O^s\, T + J^a \tag{4}$$

$$0 = \nabla O\, T + B' + J^a, \tag{5}$$

which provide the optimization method with 15 equations to solve simultaneously. The a priori state used to initialize this system is detailed in Appendix B, and all variables and

parameters are listed together with their a priori estimates and error bars in Tables 1–2.

The first right-hand side terms in Eqs. (1)–(5) are the mass and tracer transport divergence, with T the mass transports and N, P, O^s, and O the nitrate, phosphate, oxygen solubility and total oxygen concentrations on box faces, respectively. The symbol ∇ stands for the horizontal divergence operator (see Sect. 2.2.1 below). The term B, optimized by the procedure, is the net top-to-bottom biological source/sink term for nutrients and $r_{P:N}$ is a constant stoichiometric ratio used for nitrate to phosphate flux conversion (see Sect. 2.2.2 below for more details). B' is the net top-to-bottom biological source/sink term for oxygen. Hereafter in Sect. 2.2.3, B' is expressed as a function of B. Last, J^a is the air–sea abiotic oxygen source/sink term. A positive value of J^a (a source) is an oceanic oxygen uptake corresponding to a negative/downward vertical flux. J^a, optimized by the procedure, is examined in detail in Sect. 4.

The left-hand side terms are set to zero, i.e. there are no time accumulation terms explicitly represented in the model. This choice is discussed below in Sect. 2.2.4 with regard to the timescale of the model.

We now detail some key aspects of this simple model formulation.

2.2.1 Transport divergence

We assumed that tracer concentrations are better known than transports, i.e. it is the circulation which need to be better constrained to significantly improve our knowledge of the system. For the model set-up, this hypothesis ultimately leads to a linear formulation of tracer transports, which means that mass transports T are optimized while concentrations N, P, O^s, and O are not. The reader is referred to the Appendix C for more details.

2.2.2 Nutrients

The net top to-bottom biological source/sink term B, optimized by the procedure, is the integrated result of the organic matter production (nutrient sink) and remineralization (nutrient source). A negative B then relates to organic matter production. We assumed that respiration/photosynthesis and remineralization of organic matter happen at a constant stoichiometric ratio for nitrate and phosphate, $r_{P:N}$. Following Anderson (1995), we set $r_{P:N}$ to 1/16.

2.2.3 The oxygen biological source/sink term B'

For the optimization procedure to be efficient, it is necessary to relate B' to B, otherwise the nutrient conservation equations would be useless to improve our knowledge of the total oxygen budget. Broecker (1974) first introduced the concept of a conservative water mass tracer (which was then called "NO") based on fixed stoichiometric relations of non-conservative tracers. It is based on the idea that the increase

in preformed nitrate due to nitrate introduction during respiration balances the oxygen consumption. This leads to the conservation equation of preformed nitrate being a conservative tracer formulation. Preformed nitrate is given by (Pérez et al., 2005)

$$N^p = N - \mathrm{AOU}/r_{O:N}, \tag{6}$$

where AOU is the Apparent Oxygen Utilization and $r_{O:N} = 150/16$ (Anderson, 1995). Taking the difference of Eq. (4) with Eq. (5) gives the AOU conservation equation:

$$0 = \nabla \mathrm{AOU}\, T - B'. \tag{7}$$

We take the AOU out of Eq. (6) and use Eq. (2) to obtain

$$0 = -r_{O:N}\nabla N^p T + r_{O:N}\nabla N T - B'$$
$$0 = \nabla N^p T + B + B'/r_{O:N}. \tag{8}$$

Assuming that preformed nitrate is indeed a conservative tracer, we obtain $B' = -r_{O:N}B$, which allows us to link the total oxygen conservation Eq. (5) to those for nutrients N and P. We are aware that this also assumes that dissolved organic matter remineralization happens with a similar stoichiometric ratio as $r_{O:N}$. The sensitivity of the results to this assumption will be tested in Sect. 3.3.

As long as preformed nitrate is considered a conservative tracer, the oxygen solubility and total oxygen conservation Eqs. (4)–(5) could be merged into a single conservation equation for the AOU. The reason why we explicitly added the oxygen solubility in the model is for the abiotic air–sea oxygen flux J^a to be constrained by two conservation equations instead of one. Although, analytically, using these two conservation equations (oxygen solubility and total oxygen) does not add more information to the system, it provides our noisy data with a more efficient optimization of the abiotic air–sea oxygen flux.

Last, one should note that we computed the oxygen solubility as a function of temperature and salinity but that both dependencies are not explicit in the conservation Eq. (4), where we only modeled the abiotic air–sea flux J^a, primarily driven by heat fluxes. This is due to the fact that we assumed all salinity related oxygen solubility tendency terms to be below the level of the error bars for transports and conservation residuals.

2.2.4 Omitted terms and residuals

All terms which are not explicitly represented in Eqs. (1)–(5) should be accounted for in the error estimates of constraint residuals.

There are no time accumulation terms in Eqs. (1)–(5). If one considers that the relevant timescale for the budgets is the 2002–2006 period, this may seem surprising. In fact, there are no observational data that would allow us to accurately estimate tracer accumulation in our domain. We thus made the choice to account for the uncertainty of this *de facto* steady state assumption for the period 2002–2006 when

Table 3. Optimized mass transport across each face of the boxes. Transports are positive north or eastward.

Face	Mass transport (10^9 kg s^{-1} ≃ 1 Sv)
North/East (T_{ne}^{ρ})	-4.3 ± 0.4
North/West (T_{nw}^{ρ})	-13.7 ± 0.8
RR (T_{rr}^{ρ})	9.3 ± 0.7
South/East (T_{se}^{ρ})	4.8 ± 0.5
South/West (T_{sw}^{ρ})	14.1 ± 0.8

we estimated the error bars on tracer conservation equations. Assuming that tracer transport variability at OVIDE between 2002, 2004 and 2006 is the main source of uncertainty in omitting time accumulation terms (one or more of those years could lead to tracer accumulation), error bars on conservation equations have been evaluated to include the standard deviation of tracer transports across the OVIDE transects.

Some other terms are not explicitly represented in Eqs. (1)–(5). For instance, horizontal mixing due to eddies could play a significant role in tracer transports because eddies tend to carry properties away from the mean current axis (e.g. Hall et al., 2004). Fortunately, this is not the case here because all faces of the two boxes are mainly oriented perpendicularly to the main currents, and thus the eddy transport tends to be parallel to faces rather than across them (Treguier et al., 2006).

Among other missing terms are the air–sea fresh water flux and the evaporation minus precipitation mass source terms. Those have been evaluated using a surface flux dataset (OAflux and NCEP re-analysis Yu et al., 2008; Kalnay et al., 2008) and found to be significantly smaller than the a priori divergence of mass transport error bars (not shown). Also, the nitrate conservation equation does not make explicit mentions of atmospheric deposition in open ocean and coastal waters, river runoff supply or denitrification effects. Álvarez et al. (2002) provide an estimate of each of these terms north of the WOCE A25 4× cruise, which was close to the OVIDE survey. It appears that denitrification almost balances the other two processes: the small residual can thus be accounted for in the error estimate of the nitrate conservation equation used here.

Taking into account this list of terms not explicitly represented in the model, we set constraint residual error bars to 0.05 × 10^9 kg s^{-1} for mass, 10 kmol s^{-1} for nitrate, 2 kmol s^{-1} for phosphate and 100 kmol s^{-1} for both oxygen solubility and total oxygen.

3 Mass, nutrient and oxygen budgets

In this section we present results for the linear optimization of mass, nutrient and oxygen budgets.

3.1 Mass budget

Optimized mass transports are given in Table 3. The mass is conserved for each box as well as the whole domain, and it has been verified that transport estimates are consistent with those from Lherminier et al. (2010).

Top-to-bottom mass transports induce a flow across the OVIDE track of 14.1 ± 0.8 × 10^9 kg s^{-1} into the NEEB box. 9.3 ± 0.7 × 10^9 kg s^{-1} of this transport are carried to the Irminger box through the RR, while 4.8 ± 0.5 × 10^9 kg s^{-1} are exported toward the Nordic Seas through the Iceland–Scotland Ridge. In the Irminger box, the RR northward transport combines with an additional influx across the Denmark Strait of 4.3 ± 0.4 × 10^9 kg s^{-1} to balance a southwestward export through the OVIDE track of 13.7 ± 0.8 × 10^9 kg s^{-1}.

Thus, if one accounts for the OVIDE face as 100 % of the NEEB (Irminger) box mass import (export), 30 % of this are taken to (out of) the Nordic Seas, while 70 % are redistributed between both boxes through the RR.

3.2 Nutrient budget

Each of the constraints terms determined using the optimized state are given in Fig. 2a and b for nitrate and phosphate. All constraints on nutrient conservation are satisfied within the imposed error bars.

Like mass transports, it is found that about 70 % of the nitrate import from the OVIDE section are taken to the Irminger Sea through the RR, while 30 % are exported to the Nordic Seas. A residual convergence is found but with a large error estimate. The optimization method we used thus shows here its interest. With a simple residual estimate, we would not be able to determine reliably the biological term amplitude. However, our inverse model procedure does combine information from nitrate, phosphate and oxygen simultaneously to optimize the B term. This explains why for the nitrate budget B is found to be about twice as large as the transport divergence it is supposed to balance (which also leads to constraint residuals being different than zero, although budgets are closed within the constraints error bars).

Thus, for the NEEB box a nitrate transport convergence is balanced by a biological negative (sink) term of amplitude $B_s = -8.4 \pm 6.6$ kmol s^{-1}. For the Irminger box, nitrate transports also converge and the biological term has an amplitude relatively similar to the NEEB box with $B_n = -7.8 \pm 6.5$ kmol s^{-1}. Thus, for the entire domain the net biological term is significantly negative and of amplitude -16.2 ± 9.3 kmol s^{-1}. Note that phosphate figures are mostly consistent with nitrate using the constant ratio $r_{P:N}$.

The distribution of the biological terms in the two boxes thus points to the region between the OVIDE track and the Greenland–Scotland Ridge as a net producer of organic matter.
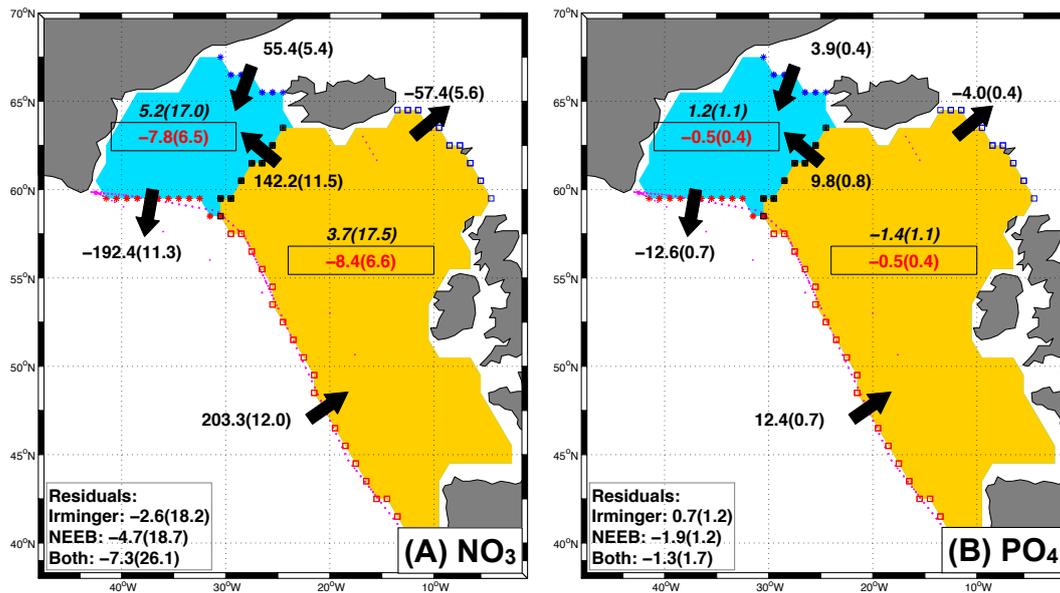
Fig. 2. (A) Nitrate and **(B)** phosphate budget terms in kmol s^{-1}. Values are net for each box – i.e. negative value reducing concentration – except for the transport through RR, which is plotted for the Irminger box (sign needs to be changed for the NEEB box). Black arrows indicate the transport direction. In the center of each box, italic values are transport divergence and framed red values are the biological net source/sink term. In the lower left corner are indicated the box and domain residuals, i.e. the left-hand sides of Eqs. (2)–(3). Values within parenthesis are error estimates.
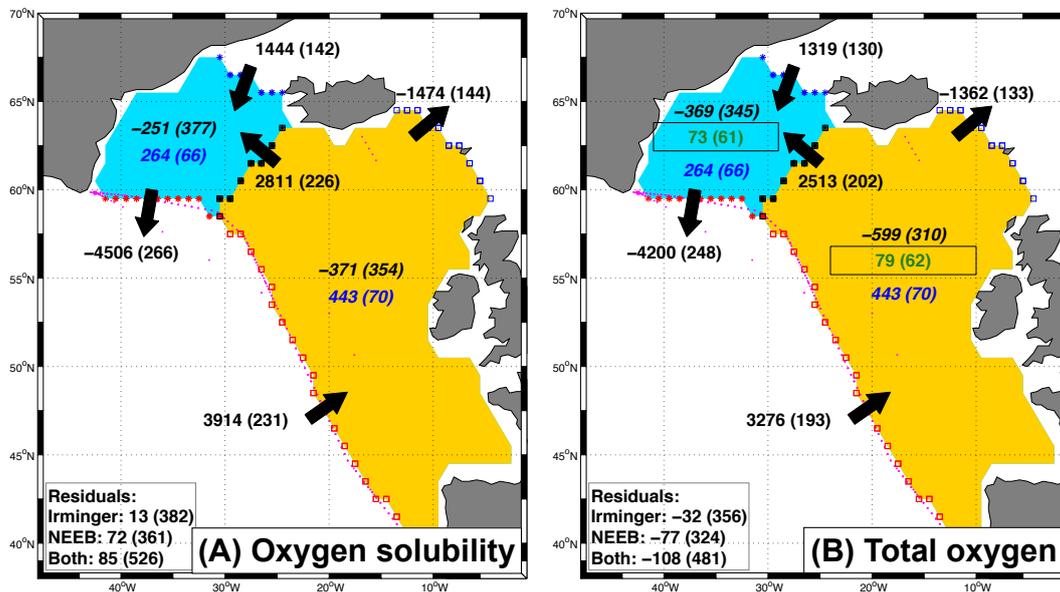
Fig. 3. (A) Oxygen solubility and **(B)** total oxygen budget terms in kmol s^{-1}. Values are net for each box – i.e. negative value reducing concentration – except for the transport through RR, which is plotted for the Irminger box (sign needs to be changed for the NEEB box). Black arrows indicate the transport direction. In the center of each box, italic values are the transport divergence, blue values are the air–sea abiotic oxygen flux (positive, downward) and framed green values are the biological net source/sink term for total oxygen. In the lower left corner are indicated the box and domain residuals, i.e. the left-hand sides of Eqs. (4)–(5). Values within parenthesis are error estimates.

3.3 Oxygen solubility and total oxygen budgets

The oxygen solubility and total oxygen budget terms determined using the optimized state are given in Fig. 3a

and b. The oxygen solubility transport terms are driven by heat transports. Therefore, it is not surprising to find a net oxygen solubility export through the OVIDE section

(-593 ± 352 kmol s^{-1}, southward) because of the net heat import into the domain (Lherminier et al., 2010). Horizontal oxygen solubility transports diverge over both boxes, which leads to an oceanic abiotic oxygen ingassing of 264 ± 66 kmol s^{-1} and 443 ± 70 kmol s^{-1} over the Irminger and NEEB boxes, respectively. We will show in Sect. 4 that this ingassing is driven by air–sea heat flux cooling, although vertical mixing due to the mixed layer dynamic does play a non-negligible role over the NEEB box.

Total oxygen transports across the OVIDE section also show a significant export (-924 ± 314 kmol s^{-1}, southward). This is due to the fact that subtropical oxygen-poor waters are transported northward (in the NEEB box), while subpolar oxygen-rich waters are transported southward (out of the Irminger box). Unlike nutrients, oxygen does show a significant southward export. Horizontal transports diverge over both boxes. This divergence is balanced by an abiotic air–sea ingassing and a net biological source term due to the photosynthesis by the phytoplankton produced in the area (see nutrient budgets). The oceanic oxygen uptake by abiotic air–sea fluxes are 264 ± 66 kmol s^{-1} and 443 ± 70 kmol s^{-1} over the Irminger and NEEB boxes, while the biological oxygen production rates are 73 ± 61 kmol s^{-1} and 79 ± 62 kmol s^{-1}. The biological source term of oxygen thus points to the region between the OVIDE track and the Greenland–Scotland Ridge as an autotrophic region. We conducted a sensitivity study of the biological oxygen term to the Redfield ratio used to relate nitrate to oxygen biological fluxes. The tested range was from $-180/14$ to $-120/18$. Although the model does show a sensitivity to the $r_{\mathrm{O:N}}$ ratio (not shown), it is largely smaller than error bars and thus cannot be isolated significantly.

4 Air–sea oxygen flux partitioning

When surface mixed layer water masses are under or over saturated in oxygen, an air–sea oxygen flux is necessary to maintain a continuous oxygen partial pressure at the air–sea interface. Under/over saturation can be due to physical and biological processes modifying the oxygen concentration of the surface layers. Therefore, the total air–sea oxygen flux can be partitioned into abiotic and biotic contributions.

The abiotic air–sea oxygen flux component is often computed using air–sea heat fluxes and thus is referred to as the thermal component (Keeling et al., 1993). However, all diabatic processes, such as air–sea heat fluxes, and also water mass mixing can change water mass temperature and thus solubility, possibly triggering abiotic air–sea oxygen fluxes. It is thus of primary interest to determine the relative contribution of air–sea heat fluxes versus mixing processes to the abiotic air–sea oxygen flux in order to test the validity of the classic method using only air–sea heat flux.

The total abiotic air–sea oxygen flux is decomposed into a thermal (θ superscript) and a mixing (H superscript) component:

$$J^{\mathrm{a}} = J^{\mathrm{a},\theta} + J^{\mathrm{a},\mathrm{H}}. \tag{9}$$

Following Keeling et al. (1993), the air–sea thermal oxygen flux can be determined as

$$J^{\mathrm{a},\theta} = -\frac{\partial \mathrm{O}_2^{\mathrm{sol}}}{\partial \theta} \frac{Q_{\mathrm{net}}}{c_{\mathrm{p}}}, \tag{10}$$

where $\mathrm{O}_2^{\mathrm{sol}}$ is the oxygen solubility (Benson and Krause Jr., 1984), c_{p} the seawater specific heat (Millard and Fofonoff, 1983) and Q_{net} the air–sea heat flux (positive upward, cooling the ocean). Using WOA09 surface averaged temperature and oxygen, we also determined the annual mean oxygen solubility dependence on temperature to be -6.9 µmol kg^{-1} °C^{-1} and -5.4 µmol kg^{-1} °C^{-1} in the Irminger and NEEB boxes.

Several methods can be used to determine the air–sea heat flux to be used in Eq. (10). The most direct one would be to use a gridded air–sea heat flux product and to compute a surface average for the two boxes. However, there are no such products with a sufficient resolution to properly resolve the East Greenland Current (EGC) and the large oceanic heat loss taking place in this western boundary current. The method we choose is in line with our study. Indeed, using optimized mass transports and temperatures from OVIDE and WOA09 data, we can compute horizontal heat transports for each of the model box faces and then define air–sea heat fluxes as their divergence. This method has the advantage of (i) being coherent with our oxygen solubility flux estimates and (ii) taking into account the heat transport by the EGC (because it is resolved by OVIDE transport estimates). We obtained horizontal heat transports in line with bibliographic standards (not shown) and we found that 221 ± 30 W m^{-2} and 72 ± 13 W m^{-2} of heat were removed from the Irminger and NEEB boxes at the surface in order to balance the heat budgets (error bars on those fluxes are from heat transport error propagation in the divergence operator).

Using these surface heat flux estimates into Eq. (10) finally leads to abiotic thermal ingassing flux estimates $J^{\mathrm{a},\theta}$ of 239 ± 65 kmol s^{-1} and 287 ± 102 kmol s^{-1} for the Irminger and NEEB boxes, respectively.

The mixing component $J^{\mathrm{a},\mathrm{H}}$ is driven by the mixed layer dynamic and the induced mixing of water masses with different temperature/salinity and oxygen properties. The nonlinear relationship between temperature (and to a lesser degree salinity) and solubility can result in the saturation of a mixed water parcel to be different than the arithmetic mean saturation of its original components, which can trigger in/outgassing (see Dietze and Oschlies, 2005, for instance). Here, we determined $J^{\mathrm{a},\mathrm{H}}$ by taking the difference of the abiotic thermal flux with the total abiotic one. We obtained an oceanic oxygen uptake by $J^{\mathrm{a},\mathrm{H}}$ of 25 ± 92 kmol s^{-1} and
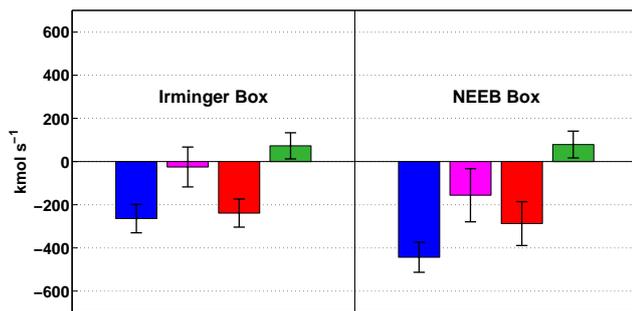
Fig. 4. Abiotic air–sea oxygen flux (kmol s^{-1}) partitioning for the Irminger (left) and NEEB (right) boxes. Note that, here, negative fluxes are into the ocean (ingassing). Blue: abiotic flux, magenta: abiotic mixing flux, red: abiotic thermal flux, and green: biological source/sink term B'. The error amplitude is represented on top of each bar.

Table 4. Abiotic air–sea oxygen flux partitioning. Fluxes are in kmol s^{-1}, positive values corresponding to ocean ingassing. For comparison, we indicated the biological source/sink term B'.

	Irminger	NEEB	Irminger+NEEB
Total abiotic (J^a)	264 ± 66	443 ± 70	707 ± 96
Thermal term ($J^{a,\theta}$)	239 ± 65	287 ± 102	526 ± 121
Mixing term ($J^{a,H}$)	25 ± 92	156 ± 123	181 ± 154
Biological term (B')	73 ± 61	79 ± 62	151 ± 87

156 ± 123 kmol s^{-1} for the Irminger and NEEB boxes, respectively.

All abiotic air–sea oxygen flux components derived here are summarized in Fig. 4 and Table 4 where we also indicated the optimized biological source/sink term B' for comparison. Over the Irminger box the abiotic air–sea oxygen flux is driven by the thermal component, presumably because of the large heat flux cooling along the EGC. Over the NEEB box, the mixing ingassing component is about half the thermal one. This shows that mixing induced air–sea oxygen fluxes can contribute significantly to the overall oceanic oxygen uptake in the region.

5 Discussion

5.1 Mass

The mass budget provides mass transport estimates through all the faces of the boxes. We note that if one accounts for OVIDE faces as 100 % of each box import/export, 30 % of these are taken to/out of the Nordic Seas while 70 % are redistributed between both boxes through RR. This simple distribution emphasizes the crucial role played by the circulation through the Reykjanes Ridge. This mass transport is the less a priori constrained and is therefore the most affected by the optimization method. That is why more observational studies are necessary for a better estimate of this circulation.

5.2 Nutrients

Because phosphate fluxes are proportional to nitrate fluxes through a constant Redfield ratio, we only discuss nitrate in the following. Nutrient transports and fluxes are thus implicitly for moles of nitrate.

Primarily because the top-to-bottom western NEEB box face is richer in nitrate than the other two faces, the nitrate optimized transports lead to a horizontal convergence in the

NEEB box. If, as hypothesized, no nitrate accumulation is taking place in the NEEB box, this convergence has to be balanced by a biological sink term (-8.4 ± 6.6 kmol s^{-1}, which corresponds to about 4 % of the western face transport). This indicates that the NEEB box is an area of nutrient biological consumption or organic matter production. Lherminier et al. (2010) determined – using the upper bound of the deep water potential density surface as a vertical limit between a surface and a deep box – that the NEEB box is primarily an upwelling region. This brings upward the deeper thermocline waters and Antarctic Bottom Water (AABW) which are rich in nutrients (McCartney et al., 1991). This large scale entrainment of deep nutrient rich water masses toward the surface layers thus suggests that the organic matter consuming nutrients in the NEEB box may be produced locally instead of being advected from the subtropical gyre water masses.

The Denmark Strait overflow and the East Greenland Current together carry 55 ± 5 kmol s^{-1} of NO$_3$ into the Irminger box while 192 ± 11 kmol s^{-1} are exported southward through the OVIDE section face. This would create a nitrate divergence in the Irminger Sea if no nitrate would have been carried in through the RR ridge. Indeed, this large flux of nitrate is able to turn the divergence into a convergence, which leads to a net biological consumption of nitrate (-7.8 ± 6.5 kmol s^{-1}) to close the budget. Like the NEEB box, the Irminger Sea is an area of organic matter production. As pointed out by Lherminier et al. (2010), the Irminger Sea is primarily a downwelling region. Thus, nutrients required for organic matter production cannot mainly originate from the local deep layers. Instead, it is likely that a large fraction of those nutrients are imported from the NEEB box through the RR.

We indicated in the introduction of this study that Álvarez et al. (2002) derived a nitrate budget for a subpolar box north of the WOCE A25 $4\times$ 1997 survey but that their transport estimates have been improved by Lherminier et al. (2007) using additional constraints based on ADCP data. So, their nitrate transport and budget have to be updated. Using these new transport estimates (Lherminier et al., 2007), we computed the nitrate transport across the WOCE A25 $4\times$ survey and obtained -16 ± 36 kmol s^{-1}, a significant reduction toward no net transport compared to the original southwestward export of -50 ± 19 kmol s^{-1}.

In our model we determined an optimized estimate for the net nitrate transport through the westernmost face of the domain (close to the WOCE A25 $4\times$ survey) of 11 ± 16 kmol s^{-1}. This figure derives from the a priori one which in turn, is the average of the 2002, 2004 and 2006 OVIDE surveys. Nitrate transports for those years are: -1 ± 49 kmol s^{-1}, 16 ± 37 kmol s^{-1} and 20 ± 32 kmol s^{-1}. Those transports show a large interannual variability. One could wonder how the budget, and especially the biological source/sink term B would be modified if more observations were available and mean values possibly modified. Using OVIDE mass and nitrate transports, we determined that the 2002–2006 mean top-to-bottom nitrate concentration on the Irminger and NEEB westernmost faces is 14 µmol kg^{-1} (see Appendix B) and has an interannual variability of about ± 1 µmol kg^{-1}. We thus performed sensitivity experiments of B_n and B_s to a priori nitrate concentrations in the range of $[13$–$15]$ µmol kg^{-1}. If the NEEB (Irminger) westernmost face nitrate concentration is increased by 1 µmol kg^{-1}, we found that the biological source/sink term decreases (increases) by 8 kmol s^{-1} because the horizontal transport convergence increases (decreases). The amplitude of the error bars on B terms (about ± 7 kmol s^{-1}) is such that this sensibility to the interannual variability of tracer concentration on the OVIDE face is barely significant. In other words, given the amplitude of a priori error bars, the interannual variability is not distinguishable from the mean state. Indeed there is no significant nitrate import through the OVIDE transect for the 2002–2006 period, and, given the amplitude of error bars, this is also the case for each of the 2002, 2004 and 2006 OVIDE surveys, and even the 1997 WOCE A25 $4\times$ survey.

5.3 Oxygen

In our model, biological source/sink terms of oxygen are directly linked to those of nutrients. Therefore, the nitrate/phosphate biological consumption by organic matter production implies a net biological production of oxygen in the two boxes through photosynthesis. Our results thus point to the region between the OVIDE track and the Greenland–Scotland Ridge as being autotrophic, with a net production of oxygen at a rate of 73 ± 61 kmol s^{-1} and 79 ± 62 kmol s^{-1} over the Irminger and NEEB boxes, respectively. Those figures were not found significantly sensitive to the Redfield ratio $r_{O:N}$. Thus, whether the autotrophy amplitude in the region is altered by the dissolved organic matter cycling or not cannot be significantly determined at this point.

Peng et al. (1987) analyzed a two-year mooring time series between March 1983 and May 1985 located at $64°$ N, $27°$ W, i.e. in the Irminger Sea. They found a seasonal cycle of biological oxygen production rate ranging from 0.3 in December to 12 mol m^{-2} yr^{-1} in May, with an annual mean of 5.1 mol m^{-2} yr^{-1}. If one attempts to extent this figure to the entire Irminger Sea, a scaling by the horizontal box surface leads to an oxygen production rate of 100 kmol s^{-1}. Our es-

timate of oxygen biological production is net, i.e. it also accounts for respiration and remineralization. Therefore, it is reassuring to find a smaller figure than the one of Peng et al. (1987).

For a better understanding of the oxygen budget in the region, we also estimated the abiotic air–sea oxygen flux and partitioned it between a thermal (due to air–sea heat flux) and a mixing (due to water mass mixing) component. The total abiotic oxygen flux ingassing estimates, scaled by the horizontal surface of each box, indicate that 5 ± 1 mol m^{-2} yr^{-1} and 13 ± 3 mol m^{-2} yr^{-1} of oxygen are fluxed into the ocean over the NEEB and Irminger boxes.

Najjar and Keeling (2000) found a thermal flux ingassing ranging from almost zero at $40°$ N to 2 mol m^{-2} yr^{-1} at $60°$ N for the Atlantic Ocean (see their Fig. 6c). Our estimates are qualitatively similar (poleward increase) but quantitatively larger: we obtained 4 ± 2 mol m^{-2} yr^{-1} and 13 ± 4 mol m^{-2} yr^{-1} for the NEEB and Irminger box thermal fluxes. This difference is probably due to the fact that they used a smooth climatology where the EGC heat loss is likely underestimated, while our estimate is based on OVIDE data that capture the large EGC heat transport. More recently, using mooring data, Körtzinger et al. (2008) found a total flux of 10 ± 3 mol m^{-2} yr^{-1} for the Labrador Sea. Although we do not have a biotic flux estimate, our abiotic flux estimate for the Irminger Sea (13 ± 3 mol m^{-2} yr^{-1}) is remarkably close to this direct observational value for the total flux.

The abiotic air–sea oxygen flux partitioning suggests that over the Irminger Sea the thermal component drives the abiotic air–sea flux. Dietze and Oschlies (2005) have shown in an eddy permitting model simulation of the North Atlantic that the annual mean abiotic oxygen flux is overestimated by the thermal flux component at high latitudes because of a mixing induced outgassing. Our results indicate that mixing induces ingassing at high latitudes (Irminger box). However, the error bar is large and the sign of this flux component is not significant in our model. On the other hand, over the NEEB box the abiotic mixing flux is significantly ingassing the ocean with oxygen. The mixing flux takes an important role in the NEEB box because of the vertical oceanic oxygen structure. In this area, there is a strong oxygen minimum around the thermocline depth, which is associated with water masses originating from the subtropical gyre and advected into the box through the southwestern face by the NAC (Van Aken et al., 1995, 1996; Sarafanov et al., 2008). Convective vertical mixing events erode and dilute these poorly saturated water masses to the surface, which result in a large mixing flux ingassing. We believe that this mechanism is robust. A poor representation of the seasonal mixed layer depth and thermocline structure in the Iceland Basin, as well as the restoration to 100% of saturation on water mass they applied on open boundaries, could explain why the Dietze and Oschlies (2005) study did not find similar conclusions. It is clear though, that further analysis is required to identify the role of mixing in air–sea oxygen fluxes.

5.4 Community production estimate

To finish this discussion, it is tempting to come back to the nutrient budget and to estimate a rate of community production of carbon. Because our budget encompasses surface and deeper processes, we are able to estimate a net community production (NCP). NCP takes place when primary production is greater than community respiration. It is an important measure of the strength of the biological pump and thus a process that must be considered in evaluating the marine cycling of carbon.

NCP, as nitrate-based carbon assimilation, can be estimated from biological source/sink terms of nitrate. Using constant stoichiometric ratios to describe the respiration/photosynthesis reactions of the marine organic matter ($C : N : P : O_2$ of $106 : 16 : 1 : -150$, see Anderson, 1995) we obtain for the Irminger and NEEB boxes NCP rates of -51 ± 43 kmolC s^{-1} and -56 ± 44 kmolC s^{-1}. The biological net consumption of nitrate producing organic matter thus indicates that the region between the OVIDE track and the Greenland–Scotland Ridge is an area of carbon fixation. It is now well known that the Redfield ratio C : N of 6.6 used here may be an underestimate (see Sambrotto et al., 1993; Toggweiler, 1993, for instance). This also seems to be the case for the northeast Atlantic open ocean (see Kahler and Koeve, 2001, discussion from the analysis of vertical profiles along the 20° W meridian between 33° N and 60° N in June/July 1996, relevant for our NEEB box). Then, if more carbon is fixed per unit of nitrate taken up – a process usually referred to as carbon over-consumption – our NCP estimates are to be considered as lower bands of the actual values.

6 Conclusions

Using a state of the art optimization method and a linear model, we combined climatological data from the WOA09 with a 2002–2006 average estimate of transports from OVIDE surveys to conserve mass, nutrients, oxygen solubility and total oxygen over the northeast Atlantic Ocean.

The optimization method used here highlights that combining climatological data with hydrographic tracers and mass transport estimates – averaged over multiple years of survey – is feasible to obtain statistically significant estimates of non-conservative tracer budget residuals. However, better sampling and improved inverse methods of the circulation of the northeast Atlantic are still required to lower error estimates both on the time average and on each individual survey. Moreover, the OVIDE surveys were conducted in late-May to mid-July and there is more summertime than wintertime data used in the derivation of the WOA09 climatology. Therefore, a seasonal bias toward late spring, early summer conditions is very likely present in our a priori state estimate. To determine the amplitude of this bias on biological source/sink terms and air–sea oxygen fluxes, future surveys should also be conducted in the wintertime. We also found that exchanges between the Irminger Sea and the Iceland Basin play a crucial role in the nutrient budgets, thus more observational estimates of the Reykjanes Ridge circulation region are required.

We successfully compared our estimates of biological and air–sea oxygen fluxes to previous studies. We determined that the region between the OVIDE survey and the Greenland–Scotland Ridge is autotrophic and is a net organic matter production region. Our quantitative estimates of the net community production of carbon could provide helpful indications to validate numerical simulations of the northeast Atlantic, where both circulation and biological models still need improvements. Also, our air–sea oxygen flux partitioning shows that the still poorly studied abiotic mixing flux component can have a very significant impact on air–sea oxygen fluxes in the presence of a strong thermocline oxygen minimum. This latter result may have implications in determining the ocean and land sinks of the atmospheric anthropic carbon with methods based on net air–sea oxygen flux estimates from the thermal component only.

Appendix A

Inverse method

Here we describe the inversion procedure used to optimize parameters of the model described in Sect. 2.2 and Appendix C. The procedure presented here is for a linear model; the reader is referred to Tarantola and Valette (1982) and Mercier (1986) for further details on a non-linear formulation.

Let $\mathbf{X} = \{X^1, ..., X^M\}$ refer to the finite set of M parameters needed to describe the system such as velocity, fluxes or tracer concentrations. A physical model will impose N constraints on the possible values of $\mathbf{X}$, which can take the functional form

$$f^1(X^1, ..., X^M) = 0$$
$$f^2(X^1, ..., X^M) = 0$$
$$...$$
$$f^N(X^1, ..., X^M) = 0.$$

Let $\mathbf{X_0}$ be an a priori state of information of the model parameters $\mathbf{X}$, and $\mathbf{E_0}$ the associated error covariance matrix. We refer to the information after inversion as the a posteriori or optimized state. The constraints take values $f(\mathbf{X})$ at $\mathbf{X}$ and their error covariance matrix is denoted as $\mathbf{E_c}$. The optimization procedure minimizes the following function:

$$(\mathbf{X} - \mathbf{X_0})^T \cdot \mathbf{E_0}^{-1} \cdot (\mathbf{X} - \mathbf{X_0}) + f(\mathbf{X})^T \cdot \mathbf{E_c}^{-1} \cdot f(\mathbf{X}), \quad \text{(A1)}$$

where the superscript T indicates a transpose operator. The first term is the squared distance between the a priori and a

posteriori estimates of the parameters, while the second term is the constraint residual weighted by their errors.

The best estimate $\mathbf{X}^*$ and its error covariance matrix $\mathbf{E}^*$ are given uniquely by

$$\mathbf{X}^* = \mathbf{X_0} - \mathbf{Q} \cdot f(\mathbf{X_0}) \tag{A2}$$
$$\mathbf{E}^* = \mathbf{E_0} - \mathbf{Q} \cdot \mathbf{F} \cdot \mathbf{E_0}, \tag{A3}$$

where $\mathbf{F}$ is the model matrix of partial derivatives (model jacobian),

$$\mathbf{F}^{ij} = \frac{\partial f^i}{\partial \mathbf{X}^j}, \tag{A4}$$

and the matrix $\mathbf{Q}$ is given by

$$\mathbf{Q} = \mathbf{E_0} \cdot \mathbf{F}^T \cdot \left(\mathbf{F} \cdot \mathbf{E_0} \cdot \mathbf{F}^T + \mathbf{E_c}\right)^{-1}. \tag{A5}$$

The set of constraints f^i used in this study are the equations Eqs. (1)–(5) written for each of the boxes and their junction (15 equations). The a priori state vector $\mathbf{X_0}$ and associated errors $\mathbf{E_0}$ are described in Appendix B and given in Table 1.

Appendix B

A priori state of the model

All variables optimized by the procedure, their values and error estimates are listed in Table 1, while fixed parameters are given in Table 2.

– **Transports across the western faces**
The western face of both boxes is defined along the OVIDE cruise track because we want to make use of the OVIDE survey data. Mass, nutrient, oxygen solubility and total oxygen transports across western faces are given by

$$T_w^C = \int\limits_{ip=1}^{n_p} \int\limits_{iz=1}^{N_l} C(ip, iz)\rho_w(ip, iz)U_w(ip, iz)\mathrm{d}S, \tag{B1}$$

where ip is a station pair and iz a vertical level. C is 1 to compute mass transports, otherwise it is the tracer transported concentration. U_w are normal absolute velocities from a ship ADCP-constrained inverse model (see Lherminier et al., 2007, 2010; Gourcuff et al., 2011). We used OVIDE tracer and velocity data available for 2002, 2004 and 2006. The list of station pair indexes to integrate over for the NEEB and Irminger box thus depends on the OVIDE cruise year. Error estimates are obtained from the error covariance matrix $\mathbf{M}(N_p, N_p)$ of the Lherminier et al. (2010) inverse model, following

$$er(T_w) = \int\int \sqrt{(C\rho_w dS)^T \cdot \mathbf{M} \cdot (C\rho_w dS)}, \tag{B2}$$

where superscript T is the transpose matrix operator. We determined mass, nutrient and oxygen transports and their associated errors for the OVIDE survey of 2002, 2004 and 2006, and then computed their time average. Because of the linear model formulation (tracer concentrations are not optimized, only mass transports are), we computed tracer concentrations along the OVIDE box faces as

$$C_w = \frac{T_w^C}{T_w^\rho} \tag{B3}$$

to keep making use of the accurate a priori tracer transport estimates from Eq. (B1).

– **Transports across the other faces**
As indicated in Appendix C, we used mean tracer and density concentrations from the WOA09 and volume fluxes from the literature:

– **Through the Denmark Strait**
Flux $F_{ne} = -4.3 \pm 2.2$ Sv is the sum of the IIC $= 0.7 \pm 0.6$ Sv (Icelandic Irminger Current, Jónsson and Valdimarsson, 2005), the EGC $= -2 \pm 1$ Sv (East Greenland Current, Pickart et al., 2005) and the DSOW $= -3 \pm 1$ Sv (Denmark Strait Overflow, Macrander et al., 2005; Dickson et al., 2008a).

– **Through the Reykjanes Ridge**
Flux $F_{rr} = 12 \pm 5$ Sv is the volume flux over the Reykjanes Ridge estimated from the range of 9.3–15.6 Sv (Treguier et al., 2005; Bower et al., 2002).

– **Through the Iceland–Scotland Ridge**
Flux $F_{se} = 4.7 \pm 2.2$ Sv is the sum of the ISI $= 7.7 \pm 2$ Sv (Iceland-Shetland Inflow: 3.8 Sv in the Faroe branch and 3.9 Sv in the Shetland branch, Hansen et al., 2008) and ISOW $= -3 \pm 1$ Sv (Iceland-Scotland Overflow: 1.9 ± 0.5 Sv at Faroe-Bank Channel and 1 ± 0.5 Sv across Iceland-Faroe, Hansen and Østerhus, 2007).

The volume flux vertical decomposition used in tracer transport estimates across the eastern face of boxes in Eq. (C2) are:

– For the Irminger box, the top layer volume flux ($F_{ne}^{top} = -0.3$ Sv) is considered to be the sum of the IIC (0.7 Sv) and half of the EGC (-1 Sv), while the bottom layer volume flux ($F_{ne}^{bottom} = -4$ Sv) is the sum of the DSOW (-3 Sv) and half of the EGC (-1 Sv). We considered the EGC to be barotropic.

– For the NEEB box, the top layer volume flux is the ISI ($F_{se}^{top} = 7.7$ Sv) and the bottom one is the ISOW ($F_{se}^{bottom} = -3$ Sv).

– **Abiotic air–sea oxygen flux**

The abiotic flux can be partitioned into a thermal and a mixing component. Because there is no estimate of the later, we estimated the former, doubled its value and associated a 200 % relative error. Following Keeling et al. (1993), the thermal flux component was computed using Eq. (10). We used the WOA09 monthly climatology of sea surface temperature and salinity to compute a monthly climatology of surface oxygen solubility and specific heat. We then used the third release of the Objectively Analyzed Air–Sea Fluxes (OAFlux) dataset (Yu et al., 2008, see http://oaflux.whoi.edu/) to compute a monthly climatology of Q_{net} for the period 1998–2007. After surface integration over each box and yearly averaging, we obtained a priori estimates of the thermal flux for the two boxes.

– **Biological source/sink terms**

The a priori estimate of B terms for the Irminger and NEEB boxes are based on observational NCP estimates from Lee (2001). They determined a regional net community production rates of 0.8 GtC yr^{-1} for the Atlantic Ocean between 40° N and 70° N. Using a surface of 12.4×10^{12} m^2 and a C : N ratio of 106 : 16, this provides a B flux estimate of 0.81 mol yr^{-1} m^{-2} for nitrate. The a priori estimate of B terms for our model was then determined by scaling this flux with the horizontal surface of the Irminger and NEEB boxes and by applying a 200 % relative error amplitude. Note that the Lee (2001) estimate is for the euphotic zone and thus should be adjusted for the top-to-bottom layer. However, we did not perform this complex adjustment because sensitivity experiments have shown that the optimized state sensibility to the a priori values of B is below the level of error bars (not shown).

– **Redfield ratios**

Following Anderson (1995), the Redfield ratios are 16 for $r_{N:P}$ and $-150/16$ for $r_{O:N}$.

Appendix C

Model details

In Sect. 2.2 we presented a synthetic formulation of the model and conservation equations. Biological source/sink terms B and abiotic air–sea fluxes J^a are straightforward terms that do not need more details. On the other hand, tracer transport divergence for a tracer C can be given more precisely by

$$\nabla C \, T = C_w \, T_w^\rho - C_e \, T_e^\rho + \alpha \, C_{rr} \, T_{rr}^\rho, \qquad (C1)$$

where C_i is 1 for mass transports, otherwise it is the mean tracer concentration on a face; T_i^ρ are mass transports across

that face; and the coefficient α is -1 for the NEEB box, 1 for the Irminger box and 0 for the entire domain.

The mass transport T_w^ρ is taken from OVIDE data while mass transports T_e^ρ and T_{rr}^ρ across the eastern and RR faces are computed as $\rho \, F$ using density ρ from the WOA09 data and volume fluxes F from literature (see details in the previous appendix).

Tracer concentrations are determined as follows:

– Along western faces C_w are computed using tracer and mass transports from OVIDE data (see Eq. B3 in the previous appendix). For a top-to-bottom estimate, this is a much better approximation than the simple face average tracer concentration.

– Along both eastern faces there is a clear two-layer current structure that the model cannot represent explicitly. If we use a simple top-to-bottom tracer concentration average with a net top-to-bottom volume flux, the a priori tracer transports across those boundaries would be badly represented. The top and bottom layer volume fluxes being known a priori, we adopted a simple method to allow for the a priori top-to-bottom tracer transports to be close to those computed using an explicit two-layer structure. Along eastern faces, C_e are computed as

$$C_e = \frac{C_e^{top}|\rho_e^{top} F_e^{top}| + C_e^{bottom}|\rho_e^{bottom} F_e^{bottom}|}{|\rho_e^{top} F_e^{top}| + |\rho_e^{bottom} F_e^{bottom}|}, \qquad (C2)$$

where "top" and "bottom" superscripts stand for the top (mainly going northward) and bottom (mainly going southward) layer properties. F are volume fluxes taken from literature, while tracer concentrations C and density ρ are computed from the WOA09 (see Table 2).

– Along the Reykjanes Ridge, we used face-averaged concentrations from the WOA09.

Finally, the tracer transport divergence term used in the model has the form

$$\nabla C \, T = C_w \, T_w^\rho - C_e \, \rho_e \, F_e + \alpha \, C_{rr} \, \rho_{rr} \, F_{rr}, \qquad (C3)$$

where only T_w^ρ, F_e and F_{rr} are optimized by the procedure so the horizontal transport divergence term remains linear.

These formulations allow for a simple top-to-bottom linear conservation model formulation making use of observational estimates while, at the same time, taking into account the basic vertical structure of water masses and circulation.

Edited by: F. Chai

The publication of this article is financed by CNRS-INSU.

References

Álvarez, M., Bryden, H., Perez, F., Rios, A., and Roson, G.: Physical and biogeochemical fluxes and net budgets in the subpolar and temperate North Atlantic, J. Mar. Res., 60, 191–226, 2002.

Álvarez, M., Ríos, A. F., Pérez, F. F., Bryden, H. L., and Rosón, G.: Transports and budgets of total inorganic carbon in the subpolar and temperate North Atlantic, Global Biogeochem. Cy., 17, 1002–1023, doi:10.1029/2002GB001881, 2003.

Anderson, L. A.: On the hydrogen and oxygen content of marine phytoplankton, Deep Sea Res. I, 42, 1675–1680, 1995.

Benson, B. and Krause Jr., D.: The concentration and isotopic fractionation of oxygen dissolved in freshwater and seawater in equilibrium with the atmosphere, Limnol. Oceanogr., 29, 620–632, 1984.

Bopp, L., Quéré, C. L., Heimann, M., Manning, A. C., and Monfray, P.: Climate-induced oceanic oxygen fluxes: Implications for the contemporary carbon budget, Global Biogeochem. Cy., 16, 1022–1045, doi:10.1029/2001GB001445, 2002.

Bower, A., Le Cann, B., Rossby, T., Zenk, W., Gould, J., Speer, K., Richardson, P., Prater, M., and Zhang, H.: Directly measured mid-depth circulation in the northeastern North Atlantic Ocean, Nature, 419, 603–607, 2002.

Brambilla, E. and Talley, L. D.: Subpolar Mode Water in the NorthEastern Atlantic. Part I: Averaged properties and mean circulation, J. Geophys. Res., 113, C04025, doi:10.1029/2006JC004062, 2008.

Brambilla, E., Talley, L. D., and Robbins, P. E.: Subpolar Mode Water in the NorthEastern Atlantic. Part II: Origin and transformation, J. Geophys. Res., 113, C04026, doi:10.1029/2006JC004063, 2008.

Broecker, W. S.: NO, a conservative water-mass tracer, Earth Planet. Sci. Lett., 23, 100–107, 1974.

de Boisséson, E., Thierry, V., Mercier, H., and Caniaux, G.: Mixed layer heat budget in the Iceland Basin from Argo, J. Geophys. Res., 115, C10055, doi:10.1029/2010JC006283, 2010.

de Boisséson, E., Thierry, V., Mercier, H., Desbruyères, D., and Caniaux, G.: Origin, formation and variability of the Subpolar Mode Water located over the Reykjanes Ridge in the ORCA025-G70 simulation, J. Geophys. Res., accepted, 2012.

Dickson, B., Dye, S., Jónsson, S., Köhl, A., Macrander, A., Marnela, M., Meincke, J., Olsen, S., Rudels, B., Valdimarsson, H., and Voet, G.: The Overflow Flux West of Iceland: Variability, Origins and Forcing. In Arctic–Subarctic Ocean Fluxes: Defining the Role of the Northern Seas in Climate., chap. 19, Springer Netherlands, 2008a.

Dickson, R. R., Meincke, J., and Rhines, P.: Arctic–Subarctic Ocean Fluxes: Defining the Role of the Northern Seas in Climate, Springer Netherlands, 2008b.

Dietze, H. and Oschlies, A.: On the correlation between air-sea heat flux and abiotically induced oxygen gas exchange in a circulation model of the North Atlantic, J. Geophys. Res., 110, C09016, doi:10.1029/2004JC002453, 2005.

Eldevik, T., Nilsen, J. E. O., Iovino, D., Anders Olsson, K., Sando, A. B., and Drange, H.: Observed sources and variability of Nordic seas overflow, Nature Geosci., 2, 406–410, 2009.

Falina, A., Sarafanov, A., and Sokov, A.: Variability and renewal of Labrador Sea Water in the Irminger Basin in 1991–2004, J. Geophys. Res., 112, C01006, doi:10.1029/2005JC003348, 2007.

Garcia, H. E., Boyer, T. P., Levitus, S., Locarnini, R. A., and Antonov, J.: On the variability of dissolved oxygen and apparent oxygen utilization content for the upper world ocean: 1955 to 1998, Geophys. Res. Lett., 32, L09604, doi:10.1029/2004GL022286, 2005.

Gourcuff, C., Lherminier, P., Mercier, H., and Le Traon, P. Y.: Altimetry combined with hydrography for ocean transport estimation, J. Atmos. Ocean. Tech., 28, 1324–1337, doi:10.1175/2011JTECHO818.1, 2011.

Hall, N. M. J., Barnier, B., Penduff, T., and Molines, J. M.: Interannual variation of Gulf Stream heat transport in a high-resolution model forced by reanalysis data, Clim. Dynam., 23, 341–351, 2004.

Hansen, B. and Østerhus, S.: Faroe Bank Channel overflow 1995–2005, Prog. Oceanogr., 75, 817–856, 2007.

Hansen, B., Østerhus, S., Turrell, W., Jónsson, S., Valdimarsson, H., Hátún, H., and Olsen, S.: The Inflow of Atlantic Water, Heat, and Salt to the Nordic Seas Across the Greenland-Scotland Ridge, in: Arctic-Subarctic Ocean Fluxes: Defining the Role of the Northern Seas in Climate, chap. 1, 15–43, Springer Netherlands, 2008.

Jónsson, S. and Valdimarsson, H.: The flow of Atlantic water to the North Icelandic Shelf and its relation to the drift of cod larvae, ICES Journal of Marine Science: Journal du Conseil, 62, 1350–1359, 2005.

Kahler, P. and Koeve, W.: Marine dissolved organic matter: can its C:N ratio explain carbon overconsumption?, Deep Sea Res. I, 48, 49–62, 2001.

Kalnay, E., Kanamitsu, M., Kistler, R., Collins, W., Deaven, D., Gandin, L., Iredell, M., Saha, S., White, G., Woollen, J., Zhu, Y., Chelliah, M., Ebisuzaki, W., Higgins, W., Janowiak, J., Mo, K. C., Ropelewski, C., Wang, J., Leetmaa, A., Reynolds, R., Jenne, R., and Joseph, D.: The NCEP-NCAR 40-year Reanalysis Project, B. Am. Meteorol. Soc., 77, 437–470, 1996.

Keeling, R. F., Najjar, R. P., Bender, M. L., and Tans, P. P.: What Atmospheric Oxygen Measurements Can Tell Us About the Global Carbon Cycle, Global Biogeochem. Cy., 7, 37–67,

doi:10.1029/92GB02733, 1993.

Körtzinger, A., Send, U., Wallace, D. W. R., Karstensen, J., and DeGrandpre, M.: Seasonal cycle of O_2 and pCO_2 in the central Labrador Sea: Atmospheric, biological, and physical implications, Global Biogeochem. Cy., 22, GB1014, doi:10.1029/2007GB003029, 2008.

Kvaleberg, E., Haine, T. W. N., and Waugh, D. W.: Middepth spreading in the subpolar North Atlantic Ocean: Reconciling CFC-11 and float observations, J. Geophys. Res., 113, C08019, doi:10.1029/2007JC004104, 2008.

Lee, K.: Global net community production estimated from the annual cycle of surface water total dissolved inorganic carbon, Limnol. Oceanogr., 46, 1287–1297, 2001.

Lherminier, P., Mercier, H., Gourcuff, C., Alvarez, M., Bacon, S., and Kermabon, C.: Transports across the 2002 Greenland-Portugal Ovide section and comparison with 1997, J. Geophys. Res., 112, C07003, doi:10.1029/2006JC003716, 2007.

Lherminier, P., Mercier, H., Huck, T., Gourcuff, C., Perez, F. F., Morin, P., Sarafanov, A., and Falina, A.: The Atlantic Meridional Overturning Circulation and the subpolar gyre observed at the A25-OVIDE section in June 2002 and 2004, Deep Sea Res. I, 57, 1374–1391, 2010.

Macrander, A., Send, U., Valdimarsson, H., Jónsson, S., and Käse, R.: Interannual changes in the overflow from the Nordic Seas into the Atlantic Ocean through Denmark Strait, Geophys. Res. Lett, 32, L06606, doi:10.1029/2004GL021463, 2005.

McCartney, M. S., Bennett, S. L., and Woodgate-Jones, M. E.: Eastward Flow through the Mid-Atlantic Ridge at 11° N and Its Influence on the Abyss of the Eastern Basin, J. Phys. Oceanogr., 21, 1089–1121, 1991.

Mercier, H.: Determining the General Circulation of the Ocean: A Nonlinear Inverse Problem, J. Geophys. Res., 91, 5103–5109, 1986.

Millard, R. J. and Fofonoff, P.: Algorithms for computation of fundamental properties of seawater, Unesco technical papers in marine science, UNESCO, 1983.

Najjar, R. G. and Keeling, R. F.: Mean Annual Cycle of the Air-Sea Oxygen Flux: A Global View, Global Biogeochem. Cy., 14, 573–584, doi:10.1029/1999GB900086, 2000.

Peng, T. H., Takahashi, T., Broecker, W. S., and Olafsson, J.: Seasonal variability of carbon dioxide, nutrients and oxygen in the northern North Atlantic surface water: observations and a model, Tellus B, 39B, 439–458, 1987.

Pèrez, F. F., Castro, C. G., Rìos, A. F., and Fraga, F.: Chemical properties of the deep winter mixed layer in the Northeast Atlantic (40–47° N), J. Marine Syst., 54, 115–125, 2005.

Pickart, R., Spall, M. A., Ribergaard, M. H., Moore, G. W. K., and Milliff, R. F.: Deep convection in the Irminger Sea forced by the Greenland tip jet, Nature, 424, 152–156, 2003a.

Pickart, R., Straneo, F., and Moore, G. W. K.: Is Labrador Sea Water formed in the Irminger basin?, Deep-Sea Res. I, 50, 23–52, 2003b.

Pickart, R. S., Torres, D. J., and Fratantoni, P. S.: The East Greenland Spill Jet, J. Phys. Oceanogr., 35, 1037–1053, 2005.

Sambrotto, R. N., Savidge, G., Robinson, C., Boyd, P., Takahashi, T., Karl, D. M., Langdon, C., Chipman, D., Marra, J., and Codispoti, L.: Elevated consumption of carbon relative to nitrogen in the surface ocean, Nature, 363, 248–250,1993.

Sarafanov, A., Falina, A., Sokov, A., and Demidov, A.: Intense warming and salinification of intermediate waters of southern origin in the eastern North Atlantic in the 1990s to mid-2000s, J. Geophys. Res., 113, C12022, doi:10.1029/2008JC004975, 2008.

Schott, F. A., Zantopp, R., Stramma, L., Dengler, M., Fischer, J., and Wibaux, M.: Circulation and Deep-Water Export at the Western Exit of the Subpolar North Atlantic, J. Phys. Oceanogr., 34, 817–843, 2004.

Sproson, D. A. J., Renfrew, I. A., and Heywood, K. J.: Atmospheric conditions associated with oceanic convection in the south-east Labrador Sea, Geophys. Res. Lett., 35, L06601, doi:10.1029/2007GL032971, 2008.

Tarantola, A. and Valette, B.: Generalized nonlinear inverse problems solved using the least squares criterion, Rev. Geophys. Space Phys., 20, 219–232, 1982.

Thierry, V., de Boisséson, E., and Mercier, H.: Interannual variability of the Subpolar Mode Water properties over the Reykjanes Ridge during 1990–2006, J. Geophys. Res., 113, C04016, doi:10.1029/2007JC004443, 2008.

Toggweiler, J. R.: Carbon overconsumption, Nature, 363, 210–211, 1993.

Treguier, A. M., Theetten, S., Chassignet, E. P., Penduff, T., Smith, R., Talley, L., Beismann, J. O., and Böning, C.: The North Atlantic Subpolar Gyre in Four High-Resolution Models, J. Phys. Oceanogr., 35, 757–774, 2005.

Treguier, A.-M., Gourcuff, C., Lherminier, P., Mercier, H., Barnier, B., Madec, G., Molines, J.-M., Penduff, T., Czeschel, L., and Böning, C.: Internal and forced variability along a section between Greenland and Portugal in the CLIPPER Atlantic model, Oc. Dyn., 56, 568–580, 2006.

van Aken, H. M. and de Boer, C.J. : On the synoptic hydrography of intermediate and deep water masses in the Iceland Basin, Deep Sea Res. I, 42, 165–189, 1995.

van Aken, H. M. and Becker, G.: Hydrography and through-flow in the northeastern North Atlantic Ocean: The NANSEN project, Prog. Oceanogr., 38, 297–346, 1996.

van Aken, H. M., Femke de Jong, M., and Yashayaev, I.: Decadal and multi-decadal variability of labrador sea water in the northwestern north atlantic ocean derived from tracer distributions: Heat budget, ventilation, and advection, Deep Sea Res. I, 58, 505–523, 2011.

Yashayaev, I.: Hydrographic changes in the Labrador Sea, 1960–2005, Prog. Oceanogr., 73, 242–276, 2007.

Yashayaev, I., Bersch, M., and van Aken, H. M.: Spreading of the Labrador Sea Water to the Irminger and Iceland basins, Geophys. Res. Lett., 34, L10602, doi:10.1029/2006GL028999, 2007.

Yu, L., Jin, X., and Weller, R. A.: Multidecade Global Flux Datasets from the Objectively Analyzed Air-sea Fluxes (OAFlux) Project: Latent and Sensible Heat Fluxes, Ocean Evaporation, and Related Surface Meteorological Variables, Tech. rep., Woods Hole Oceanographic Institute, 2008.